MBoC | ARTICLE

A fine balance among key biophysical factors is required for recovery of bipolar mitotic spindle from monopolar and multipolar abnormalities

Xiaochu Li[a,b], Mathew Bloomfield[a,c], Alexandra Bridgeland[c,d], Daniela Cimini[a,c] and Jing Chen[a,c,e,*]

[a]Department of Biological Sciences, [b]BIOTRANS Graduate Program, [c]Fralin Life Sciences Institute, [d]Systems Biology Program, College of Science, and [e]Center for Soft Matter and Biological Physics, Virginia Tech, Virginia Tech, Blacksburg, VA 24061

ABSTRACT **During mitosis, equal partitioning of chromosomes into two daughter cells requires assembly of a bipolar mitotic spindle. Because the spindle poles are each organized by a centrosome in animal cells, centrosome defects can lead to monopolar or multipolar spindles. However, the cell can effectively recover the bipolar spindle by separating the centrosomes in monopolar spindles and clustering them in multipolar spindles. To interrogate how a cell can separate and cluster centrosomes as needed to form a bipolar spindle, we developed a biophysical model, based on experimental data, which uses effective potential energies to describe key mechanical forces driving centrosome movements during spindle assembly. Our model identified general biophysical factors crucial for robust bipolarization of spindles that start as monopolar or multipolar. These factors include appropriate force fluctuation between centrosomes, balance between repulsive and attractive forces between centrosomes, exclusion of the centrosomes from the cell center, proper cell size and geometry, and a limited centrosome number. Consistently, we found experimentally that bipolar centrosome clustering is promoted as mitotic cell aspect ratio and volume decrease in tetraploid cancer cells. Our model provides mechanistic explanations for many more experimental phenomena and a useful theoretical framework for future studies of spindle assembly.**

Monitoring Editor
Alex Mogilner
New York University

Received: Nov 2, 2022
Revised: Jun 12, 2023
Accepted: Jun 15, 2023

INTRODUCTION

During mitosis, assembly of the bipolar mitotic spindle is essential for faithful segregation of the duplicated chromosomes into two daughter cells (Walczak and Heald, 2008; Prosser and Pelletier, 2017). Nonbipolar spindles can lead to chromosome missegregation and chromosome number abnormalities in the daughter cells, which may cause cell death or abnormal cell behaviors, including those implicated in diseases such as cancer (Silkworth and Cimini, 2012; Vitre and Cleveland, 2012).

Mitotic spindle assembly is a tightly orchestrated process, in which the microtubule (MT) network in the cell undergoes dramatic reorganization under the joint activity of a large number of molecular motors and regulatory molecules (Walczak and Heald, 2008; Prosser and Pelletier, 2017). During this process, a pair of large multiprotein organelles called "centrosomes" (CSs) play a crucial role in organizing the MT arrays and forming the two poles of the mitotic spindle (Hoffmann, 2021). Aberrancies in the activity, number and structure of the CSs and their functionally associated cellular components can cause defective spindle assembly, especially formation of monopolar and multipolar spindles (Hinchcliffe and Sluder, 2001; Godinho and Pellman, 2014). A monopolar spindle can be caused by defects in CS duplication, motor-dependent forces, or MT dynamics (Tillement *et al.*, 2009). It can also be induced experimentally by chemical inhibitors of the Eg-5 motors that mediate antiparallel sliding of MTs and CS separation (Mayer *et al.*, 1999; Kapoor *et al.*, 2000; Skoufias *et al.*, 2006). A persisting monopolar spindle can lead to aberrant mitotic exit and cell death (Hu *et al.*, 2008; Tillement *et al.*, 2009). Although multipolar spindles can assemble

This article was published online ahead of print in MBoC in Press (http://www.molbiolcell.org/cgi/doi/10.1091/mbc.E22-10-0485) on June 21, 2023.

*Address correspondence to: Jing Chen (chenjing@vt.edu).

Abbreviations used: CS, centrosome; Inter-CS, intercentrosomal; MT, microtubule; SEM, standard error of the mean; SD, standard deviation.

due to other defects (Maiato and Logarinho, 2014), the presence of supernumerary CSs, which is a common feature of cancer cells, often leads to multipolar spindle assembly (Chan, 2011; Godinho and Pellman, 2014). When multipolar cell division ensues, the daughter cells usually suffer from fatal aneuploidy (Ganem *et al.*, 2009; Baudoin *et al.*, 2020).

Interestingly, the spindle assembly process is rather robust and can often rescue itself from monopolar and multipolar abnormalities over the course of mitosis. For example, the spindle can effectively recover bipolarity from monopolarity induced by an Eg-5 inhibitor after the drug is washed out (Kapoor *et al.*, 2000; Khodjakov *et al.*, 2003; Lampson *et al.*, 2004). Similarly, cells can cluster supernumerary CSs into two poles to preserve spindle bipolarity (Quintyne *et al.*, 2005; Ganem *et al.*, 2009; Silkworth *et al.*, 2009; Baudoin *et al.*, 2020). In fact, CS clustering provides an important way for cancer cells with supernumerary CSs to avoid lethal multipolar division, albeit at the cost of an elevated rate of minor, survivable chromosome missegregation. The latter is implicated in development of chromosomal instability that drives carcinogenesis (Ganem *et al.*, 2009; Silkworth *et al.*, 2009; Ogden *et al.*, 2012; Silkworth and Cimini, 2012; Milunovic-Jevtic *et al.*, 2016).

Rescue from either the monopolar or multipolar abnormality is mediated largely by the same molecules that mediate formation of bipolar spindles in a typical mitosis. How does the spindle assembly mechanism then operate such that it can rescue both the monopolar and multipolar abnormalities? In other words, how does the mechanism manage to separate and cluster the CSs, depending on needs, and effectively achieve a bipolar spindle under different perturbations?

In this work, we addressed the above question by combining biophysical modeling and experiments. Many previous modeling studies have addressed the dynamics and mechanics of spindle assembly in different model organisms, often focusing on specific aspects of the process, such as CS separation (Cytrynbaum *et al.*, 2003; Blackwell *et al.*, 2017), spindle positioning (Kozlowski *et al.*, 2007; Som *et al.*, 2019), spindle bipolarity (Blackwell *et al.*, 2017; Lamson *et al.*, 2019; Chatterjee *et al.*, 2020; Edelmaier *et al.*, 2020), MT alignment (Hepperla *et al.*, 2014; Mirabet *et al.*, 2018; Lamson *et al.*, 2019; Edelmaier *et al.*, 2020), MT-chromosome attachment (Burbank *et al.*, 2007; Paul *et al.*, 2009), and chromosome oscillation (Civelekoglu-Scholey *et al.*, 2006; Liu *et al.*, 2007, 2008; Civelekoglu-Scholey *et al.*, 2013). Unlike most of these models, which resolve the dynamics of individual MTs, motors, crosslinkers, and so forth, here we built a parsimonious model that uses effective potential energies to characterize general types of forces that drive the movements of CSs in the mitotic cell. The model was parametrized through combining the measured timing of separation of two CSs in normal mitoses after washout of the Eg-5 inhibitor and existing quantitative data on the molecular players in spindle assembly (e.g., typical magnitude of force generated by MT-associated motors and typical size of spindle; see Supplemental Table S1). The parsimonious model allowed us to predict general biophysical factors that are crucial for robust rescue of the bipolar spindle from monopolar and multipolar abnormalities. We found that intercentrosomal (inter-CS) force fluctuation with proper intensity and timescale is essential for CS separation and CS clustering in rectifying monopolarity and multipolarity, respectively. Effective CS clustering is further promoted by a balance between inter-CS attractive and repulsive interactions, rounding and shrinking of the cell, exclusion force driving CSs away from the center of the cell, and a smaller number of CSs. Particularly, our predictions about cell geometry and size were validated by our experimental observations in tetraploid DLD-1 cancer cells. Other predictions also provide explanation for a number of intriguing observations reported in the literature. Overall, our model provides critical physical insights and testable predictions for the key factors that ensure robustness and flexibility in mitotic spindle assembly.

MODEL

Effective potential energies

The ultimate spindle state, whether bipolar, monopolar, or multipolar, depends on movement of the CSs in the cell. Movement of the CSs is driven by complex mechanical interactions mediated by the MTs, molecular motors, chromosomes, and other MT-associated proteins (Gergely and Basto, 2008; Walczak and Heald, 2008; Kramer *et al.*, 2011; Marthiens *et al.*, 2012; Prosser and Pelletier, 2017; Elting *et al.*, 2018) (Figure 1A). In this work, we built a parsimonious biophysical model, in which the mechanical interactions are approximated by two types of potential energies. The first type comprises interactive potential energies between each pair of CSs (inter-CS energies), and the second type consists of potential energies between the CS and other cellular components, which effectively drive CS movements along the radii of the cell (radial energies) (Figure 1B). The simplified representation of mechanical interactions allows us to focus on the most essential physical factors contributing to bipolar spindle formation, without detailing the specific molecular players.

Inter-CS energy. An inter-CS energy between a pair of CSs recapitulates all the direct and indirect mechanical interactions between the two CSs (Figure 1A). These mechanical interactions can be attractive or repulsive. Attractive forces are typically generated by minus-end directed molecular motors (e.g., kinesin-14 motors [Cai *et al.*, 2009; Hepperla *et al.*, 2014; She and Yang, 2017]) acting on the MTs connecting two CSs (Figure 1A, large brown arrows). Attraction can also occur between two CSs attached to the same chromosomal kinetochore, as MTs extending from the same kinetochore tend to align (Figure 1A, small brown arrows; Goshima *et al.*, 2005). Similarly, repulsive forces are typically generated by plus-end directed motors (e.g., Eg-5 [Kapitein *et al.*, 2005; Tanenbaum and Medema, 2010]) acting on the MTs connecting two CSs (Figure 1A, large blue arrows). Repulsion can also act between CSs attached to opposing sister kinetochores on a chromosome through the torque that orients the sister kinetochores back to back and points their associated MT bundles oppositely (Figure 1A, small blue arrows; Paul *et al.*, 2009; Miles *et al.*, 2022). Instead of detailing the molecular players and their dynamics, we depict the overall effect of the inter-CS mechanical interactions between any two CSs as a potential energy that depends on the distance between the CSs (Figure 1, B and C). Particularly, net attraction between the CSs occurs over short inter-CS distances and net repulsion occurs over long inter-CS distances (Figure 1C). Such a general setting is essential for bipolar spindle formation, because the alternative general setting, with net repulsion over short distances and net attraction over long distances, would drive the CSs into a "cloud" where all the CSs are spaced roughly at the energy-minimum distance between each other (Supplemental Figure S1), rather than forming a bipolar spindle. For simplicity, we express the inter-CS energy in a general form as Eq. 1.

$$\Phi_{c,ij} = \begin{cases} K_a L_a \left(1-\exp\left(-\frac{d_{ij}}{L_a}\right)\right) + K_r L_r \left(1-\exp\left(-\frac{L_d - d_{ij}}{L_r}\right)\right), & \text{if } 0 \le d_{ij} \le L_d \\ K_a L_a \left(1-\exp\left(-\frac{L_d}{L_a}\right)\right), & \text{if } d_{ij} > L_d \end{cases} \quad (1)$$

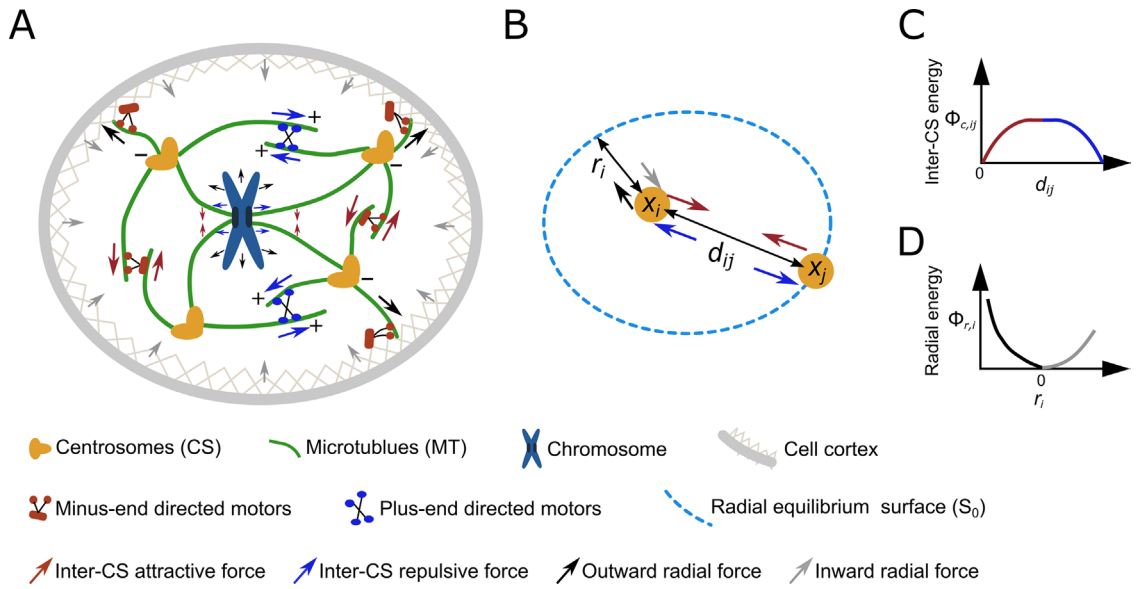

FIGURE 1: Effective potential energies that drive spindle assembly. (A) Cartoon summary of key cellular components contributing to spindle assembly. The cartoon exemplifies a cell with four CSs. MTs connect the CSs, chromosomes, and cell cortex, with MT-associated motors exerting pushing and pulling forces among them. (B) Forces exerted on a CS by other CSs and other cellular components. Inter-CS forces are assumed to depend on the inter-CS distance, d_{ij}. The radial forces position the CS preferably underneath the cell cortex but outside the chromosome mass. The inward and outward radial forces are assumed to cancel each other out at a radial equilibrium surface (blue dashed line). (C and D) Effective potential energy profiles for the inter-CS (C) and radial forces (D). Red and blue legs in (C) represent attractive and repulsive zones, respectively, in the inter-CS interaction. Black and gray legs in (D) represent zones with net outward and inward forces, respectively, on the CS.

In Eq. 1, $\Phi_{c,ij}$ is the inter-CS potential energy between the i-th and j-th CSs. d_{ij} is the distance between the two CSs. K_a and K_r are the intensities of the attractive and repulsive forces, respectively. L_a and L_r are the characteristic ranges of the attraction and repulsion, respectively. L_d is the maximum distance over which two CSs can interact with each other. This is a convenient assumption that prevents the repulsive energy well from becoming too deep when the size of the cell changes. Nevertheless, L_d is qualitatively related to the biophysical limitations of MTs and MT-associated motors.

The inter-CS force is obtained by taking the derivative of the inter-CS energy with respect to the inter-CS distance (Eq. 2).

$$F_{c,ij} = -\frac{d\Phi_{c,ij}}{dd_{ij}} = \begin{cases} -K_a \exp\left(-\frac{d_{ij}}{L_a}\right) + K_r \exp\left(-\frac{L_d - d_{ij}}{L_r}\right), & \text{if } 0 \le d_{ij} \le L_d \\ 0, & \text{if } d_{ij} > L_d \end{cases} \tag{2}$$

Radial energy. During spindle formation, the CSs are typically located in the space between the cell cortex and the chromosome mass (Manneville and Etienne-Manneville, 2006). Such a spatial constraint is initiated before nuclear envelope breakdown and continues throughout mitosis. Mechanistically, the spatial constraint is mediated by the following processes: 1) the CSs are spatially confined by the cell cortex (Figure 1A, gray arrows); 2) the dyneins associated with the cell cortex attach to the astral MTs emanating from a CS and pull the CS toward the cell cortex (Elting *et al.*, 2018; Figure 1A, large black arrows); and 3) the chromosomes and nuclear components occupy the central region of the cell and exert a steric exclusion on the CSs (Figure 1A, small black arrows). The cortical confinement force points inward from the cell boundary; the cortical pulling forces and chromosome exclusion forces both point outward. These inward and outward forces are captured by a potential energy along the radial direction (Figure 1, B and D). This radial energy positions the CSs preferably beneath the cell cortex, yet outside the chromosome mass. It is assumed to be a function of the distance of the CS from an effective "radial equilibrium surface," S_0, on which the inward and outward forces equate (Figure 1B, blue dashed ellipse). In this work, the cell shape is assumed to be an oblate spheroid, which is consistent with typical observations in cultured mitotic cells (Magidson *et al.*, 2011; Charnley *et al.*, 2013; Lancaster *et al.*, 2013). The radial equilibrium surface follows a similar geometry and is mathematically defined by Eq. 3, where the equatorial radius a is smaller than but close to the cell radius from the top view, and the polar axis length c is smaller than but close to the cell height.

$$\frac{x^2}{a^2} + \frac{y^2}{a^2} + \frac{z^2}{c^2} = 1 \tag{3}$$

The radial potential energy is expressed as a piecewise function of the shortest distance of the CS to the radial equilibrium surface (Eq. 4).

$$\Phi_{r,i} = \begin{cases} \frac{1}{2}K_{in}(r_i)^2, & \text{if } r_i \ge 0; \\ \frac{1}{2}K_{out}(r_i)^2, & \text{if } r_i < 0 \end{cases} \tag{4}$$

In Eq. 4, K_{in} and K_{out} are intensities of the inward and outward forces, respectively, and r_i is the shortest distance of the i-th CS to the radial equilibrium surface. The sign of the distance indicates whether the CS is inside (negative) or outside (positive) the radial equilibrium surface.

The radial force on the i-th CS is obtained by taking the derivative of the radial potential energy with respect to r_i (Eq. 5). When the

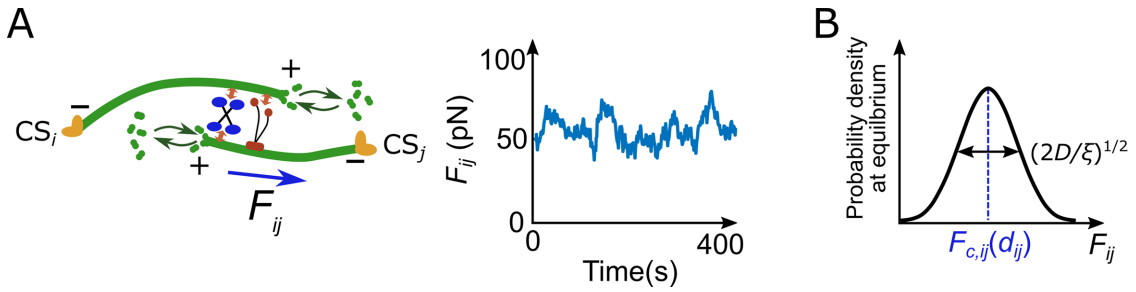

FIGURE 2: Inter-CS force fluctuation. (A) MT instability and dynamics of the MT-associated motors (cartoon on the left) cause temporal fluctuations in the inter-CS forces (example time plot on the right). (B) Equilibrium probability distribution of the fluctuating inter-CS force if the inter-CS distance were fixed. Temporal fluctuation of the inter-CS force follows the Langevin dynamics in Eq. 6. If the inter-CS distance were fixed, the force would follow a Gaussian distribution with mean value $F_{c,ij}(d_{ij})$ described by Eq. 2 and SD $\sqrt{2D/\xi}$.

CS is outside the radial equilibrium surface ($r_i \geq 0$), the radial force points inward (negative). When the CS is inside the radial equilibrium surface ($r_i < 0$), the radial force points outward (positive).

$$F_{r,i} = -\frac{\partial \Phi_{r,i}}{\partial r_i} = \begin{cases} -K_{in} r_i, & \text{if } r_i \geq 0; \\ -K_{out} r_i, & \text{if } r_i < 0 \end{cases} \tag{5}$$

Temporal fluctuations in inter-CS forces

Spindle formation involves highly dynamic molecular processes, such as MT instability and random binding/unbinding of motors with the MTs. These dynamic processes are essential for separation of CSs and establishment of antiparallel MT arrays (Nedelec, 2002; Cytrynbaum *et al.*, 2003; Ferenz *et al.*, 2009; Hepperla *et al.*, 2014; Blackwell *et al.*, 2017; Mirabet *et al.*, 2018; Lamson *et al.*, 2019; Edelmaier *et al.*, 2020). Because of these dynamic molecular processes, the inter-CS force constantly fluctuates over time (Figure 2A). We hence introduce stochastically fluctuating dynamics in the inter-CS force via Eq. 6.

$$\dot{F}_{ij}(t) + \xi\left(F_{ij}(t) - F_{c,ij}(t)\right) + \varepsilon(t) = 0 \tag{6}$$

In Eq. 6, $F_{ij}(t)$ is the instantaneous inter-CS force. $F_{c,ij}(t)$ is the mean inter-CS force determined by the inter-CS potential energy (Eq. 2). ξ is the relaxation rate constant of the force fluctuation. The noise term $\varepsilon(t)$ obeys the Gaussian distribution with the correlation function $\langle \varepsilon(t)\varepsilon(t')\rangle = 2D\delta(t-t')$, where $\delta(t-t')$ is the Dirac delta function and D is the level of force fluctuation. If an inter-CS distance is fixed, the fluctuating force would assume a Gaussian distribution (Figure 2B). Note that addition of the inter-CS force fluctuation to the model is necessary to recover the bipolar spindle from the monopolar state (Figure 3, B and C). We chose parameters for the force fluctuation (Supplemental Table S1) such that the time needed for initiating and completing CS separation in model simulations roughly matched those observed experimentally (Supplemental Figure S2; Supplemental Movie S1).

Equation of motion for CSs

Motion of each CS under the influence of the inter-CS and radial forces is governed by the Langevin equation given by Eq. 7.

$$\dot{\boldsymbol{x}}_i(t) = \frac{1}{\gamma}\left(F_{r,i}\boldsymbol{u}_{r,i} + \sum\nolimits_{j\neq i} F_{ij}\boldsymbol{u}_{ij}\right) + \boldsymbol{\eta}(t) \tag{7}$$

In Eq. 7, $\boldsymbol{x}_i(t) = \left[x_i(t),\, y_i(t),\, z_i(t)\right]$ is the position of the i-th CS at time t. $\dot{\boldsymbol{x}}_i(t) = \left[\dot{x}_i(t),\, \dot{y}_i(t),\, \dot{z}_i(t)\right]$ is the velocity of the i-th CS. $\boldsymbol{u}_{r,i}$ is the unit vector representing the direction of $F_{r,i}$; it points from $\boldsymbol{x}_i$ toward the point on the radial equilibrium surface that has the shortest distance from $\boldsymbol{x}_i$. $\boldsymbol{u}_{ij} = \left(\boldsymbol{x}_i - \boldsymbol{x}_j\right)/d_{ij}$ is the unit vector representing the direction of F_{ij}; it points from the j-th CS to the i-th CS. The noise term $\boldsymbol{\eta}(t) = \left[\eta_1(t),\, \eta_2(t),\, \eta_3(t)\right]$ obeys the Gaussian probability distribution with the correlation function $\left\langle \eta_p(t)\eta_q(t')\right\rangle = \frac{2k_BT}{\gamma}\delta_{pq}\delta(t-t')$, where $p, q = 1, 2, 3, \delta_{pq}$ is the Kronecker delta function, and $\delta(t-t')$ is the Dirac delta function. γ is the effective drag coefficient of the CS (with the associated MTs). k_BT is the thermal energy. Incorporation of γ in the noise term follows from the fluctuation–dissipation theorem (Landau and Lifshitz, 1996). $F_{r,i}$ and F_{ij} are computed using Eqs. 5 and 6, respectively. Note that the inter-CS force fluctuation is applied solely in the direction of the force, because this fluctuation is presumably caused by fluctuations in the activities of motors, MTs, and other components that exert the force.

RESULTS

Inter-CS force fluctuation with proper intensity and timescale is essential for recovering bipolar spindle from monopolar state

We first investigated recovery of a bipolar spindle from the monopolar state in a cell with two CSs (Figure 3A). We ran 2-h simulations of the model, starting with the two CSs close together (Supplemental Movie S1). Depending on the time trajectory of the inter-CS distance, three types of behaviors can be found (Supporting Materials and Methods): 1) Stable bipolar: the CSs are fully separated to form a bipolar spindle that persists for a long time (Figure 3A, green trajectory). 2) Monopolar: the CSs are never separated in 2 h (Figure 3A, red trajectory). 3) Unstable: the CSs are separated only transiently, with frequent conversions of the spindle between bipolarity and monopolarity (Figure 3A, blue trajectory).

Our model results show that a proper level of inter-CS force fluctuation is the key to bipolar spindle recovery from the monopolar state. Without the inter-CS force fluctuation, the spindle is stuck in the initial monopolar state (Figure 3, B and C), unless the inter-CS force intensity is very low (Figure 3B, bottom left corner). In the latter case, however, the bipolar spindle is unstable and hence cannot execute its function in mitosis (Figure 3B). These results can be understood as follows. The CSs are initially close to each other, that is, they start in the attraction zone in the inter-CS energy profile (Figure 1C, red leg). Without inter-CS force fluctuation, the intrinsic thermal fluctuation of the CSs (i.e., $\boldsymbol{\eta}(t)$ in Eq. 7, which is quite small because it is physically constrained by γ, the effective drag coefficient of the CS and its associated MTs) is not sufficient to drive the CSs out of the attraction zone. This is true unless the inter-CS force intensity is very low, which corresponds to a very low energy barrier between the attraction and repulsion zones. With a very low energy barrier,

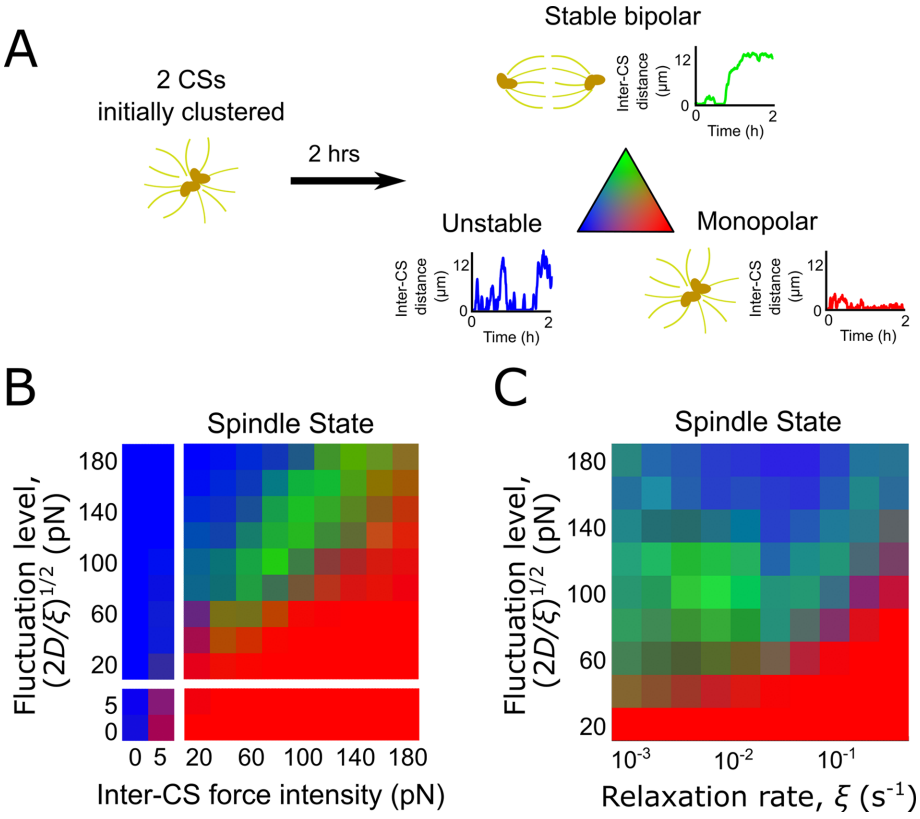

FIGURE 3: Effects of inter-CS force fluctuation on bipolar spindle recovery with two CSs. (A) Schematic representation of simulation and result analysis. Each simulation started with the two CSs in a cell close to each other, mimicking a monopolar state induced by Eg-5 inhibition. Movements of CSs were simulated for 2 h. The spindle dynamics can be categorized into three types: stable bipolar, monopolar, and unstable. Detailed method for determining the spindle state from the simulation data is described in Supporting Materials and Methods. (B and C) Model predicted fractions of three spindle states with varied inter-CS force fluctuation level versus varied inter-CS force intensity (B), and with varied inter-CS force fluctuation level versus varied relaxation rate constant for the inter-CS force fluctuation (C). Thirty stochastic simulations were performed for each parameter set. The fraction of each spindle state for a given parameter set is color coded according to the color triangle given in (A). In (B), attractive and repulsive force intensities change by the same amount, with the attractive force intensity always 40 pN smaller than the repulsive force intensity, as in the default parameter set (Supplemental Table S1); this asymmetry is necessary for forming a stable bipolar spindle (Supplemental Figure S3). The *x*-axis shows the attractive force intensity K_a.

however, the system would quickly jump back and forth between the attraction and repulsion zones, rendering the bipolar spindle unstable. Increasing the inter-CS force fluctuation adds a constant perturbation to the system and helps the CSs escape the attraction zone. But if the inter-CS force fluctuation is too strong compared with the inter-CS force intensity, the fluctuation can also induce frequent crossing of the energy barrier between the attraction and repulsion zones and make the bipolar spindle unstable (Figure 3B). As the inter-CS force intensity increases, a stronger force fluctuation is needed to get the system out of the monopolar state (Figure 3B). Taken together, a proper level of inter-CS force fluctuation relative to the inter-CS force intensity is necessary for stable bipolar spindle recovery from the monopolar state.

Proper relaxation rate of the inter-CS force fluctuation is also important for recovering a stable bipolar spindle from the monopolar state. The relaxation rate constant ξ in Eq. 6 depicts how fast the inter-CS forces randomly rise and fall. The model predicts an optimal relaxation rate constant around 10^{-2} s^{-1}, which, in combination with a proper fluctuation level, gives rise to a "sweet spot" with the highest fraction of stable bipolar spindles (Figure 3C, green area). Indeed, the timescales associated with MT instability and binding/unbinding dynamics of MT-associated motors—the source of inter-CS force fluctuation—fall in the range of tens of seconds (Verde *et al.*, 1992; Belmont and Mitchison, 1996; Valentine *et al.*, 2006; Gardner *et al.*, 2011; Kunwar *et al.*, 2011; Norris *et al.*, 2018; Reinemann *et al.*, 2018), consistent with the optimal relaxation rate predicted for inter-CS force fluctuation. Overall, these results indicate that inter-CS force fluctuation with proper intensity and timescale is crucial for recovering a stable bipolar spindle from the monopolar state.

Balance between inter-CS attraction and repulsion is required for bipolar CS clustering

We next turned to the CS clustering process in a cell with supernumerary CSs. In the next few subsections, we will report the model-predicted effects of various biophysical factors in a cell with four CSs (because cells that undergo whole genome doubling—a frequent event in tumor evolution [Lens and Medema, 2019]—will enter mitosis with four CSs). However, it is worth noting that our findings about these biophysical factors hold true for different numbers of extra CSs.

For a cell with four CSs, we ran 2-h simulations with the CSs randomly scattered in the cell at the initial time (Figure 4A; Supplemental Movie S2). We classified the results into three types based on the number of spindle poles at the end of a simulation: 1) monopolar, 2) bipolar, and 3) multipolar (Figure 4A, Supporting Materials and Methods). Stability of the states will be plotted separately in the cases that warrant a discussion of it.

The model reveals opposite effects imposed by the inter-CS attraction and repulsion on the spindle state. Stronger attraction promotes monopolarity (Figure 4B, red area), because in this case, the CSs tend to enter and stay in the deep attraction zone of the inter-CS potential energy (Figure 1C). Conversely, stronger repulsion encourages multipolarity (Figure 4B, blue area), because the CSs are more likely to stay in the deep repulsive energy well at the far end of the inter-CS potential energy (Figure 1C). Bipolarity is favored when the attractive force scales with the repulsive force (Figure 4B, green area).

In addition, sufficient levels of both attraction and repulsion between CSs are necessary for forming a stable bipolar spindle. When inter-CS attraction and repulsion are too low, even if they scale with each other and spindle bipolarity occurs with a substantial frequency, most of these bipolar spindles are unstable (Figure 4C; Supplemental Figure S4) and cannot stay bipolar for ≥30 min (Supporting Materials and Methods). This is because random fluctuations (both intrinsic fluctuations and fluctuations in the inter-CS forces) can easily bring the system out of the shallow energy wells.

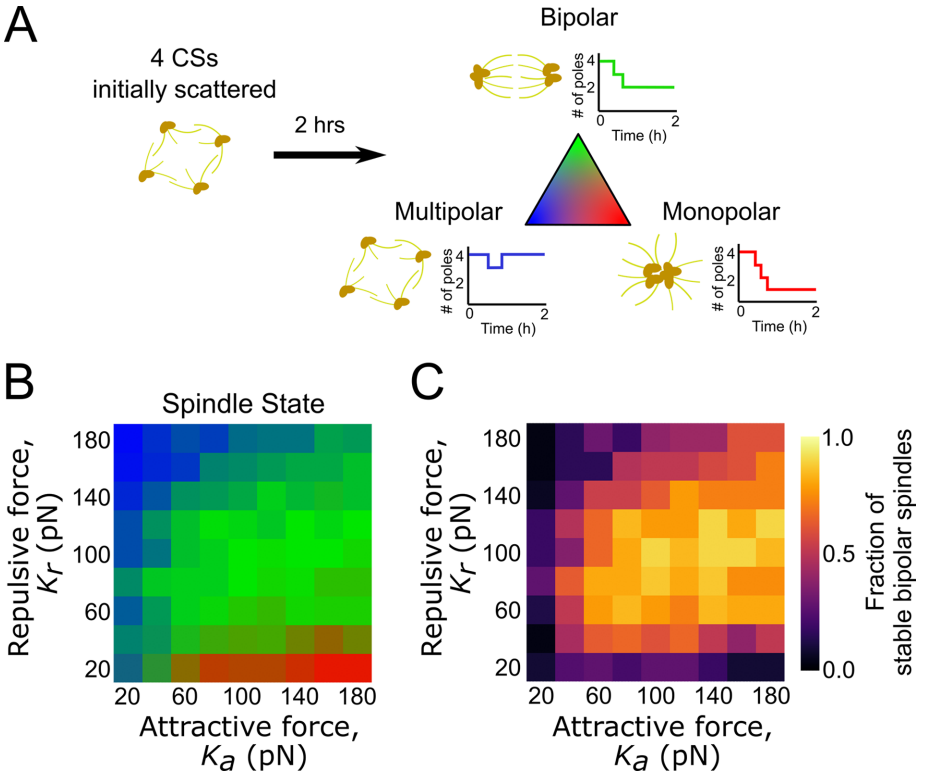

FIGURE 4: Effects of inter-CS attraction and repulsion on spindle formation with four CSs. (A) Schematic representation of simulation and result analysis. Each simulation started with four CSs randomly scattered, and CS movement was simulated for 2 h. At the end of the simulation, the spindle can assume the bipolar, multipolar, or monopolar state. Detailed method for determining the spindle state from the simulation data is described in Supporting Materials and Methods. (B) Model predicted fractions of three spindle states with varied inter-CS attractive and repulsive force intensities. The fraction of each spindle state for a given parameter set is color coded according to the color triangle given in (A). (C) Model predicted fraction of stable bipolar spindle (in all simulations) with varied inter-CS attractive and repulsive force intensities. Thirty stochastic simulations were performed for each parameter set.

Overall, we found that formation of stable bipolar spindle requires sufficient and balanced inter-CS attraction and repulsion. Note that, similar to the system with two CSs, a multi-CS system also requires a balance between the inter-CS force intensity and force fluctuation level for effective bipolar spindle formation (Supplemental Figure S5). However, the spatial ranges of inter-CS attraction and repulsion do not have a significant effect on the spindle state (Supplemental Figure S6A).

Cell rounding facilitates bipolar CS clustering while slight flatness guides spindle orientation

We then explored the effect of cell geometry on CS clustering. We ran simulations with the same settings as those described in the previous section but assigned different aspect ratios and a fixed volume to the model cell. Interestingly, the model reveals that a rounder cell geometry facilitates bipolar spindle formation (compare Figure 5, A and B, with Figure 4, B and C). Compared with a perfectly round geometry (Figure 5A) or the default, slightly flat geometry that is typically observed in cultured cells (Figure 4B), severely flat cells are predicted to suffer significantly lower fraction of bipolar spindles and higher fraction of multipolar spindles across the range of inter-CS attractive and repulsive force intensities (Figure 5B). The fraction of stable bipolar spindles is also significantly lower in severely flat cells (Figure 5B) than in rounder cells (Figures 4C and 5A). When the spatial ranges of inter-CS attraction and repulsion vary, the model also predicts a low fraction of bipolar spindles and high fraction of multipolar spindles in severely flat cells (Supplemental Figure S6C), whereas the fraction of bipolar spindles stays high for most values of spatial ranges with the default and round geometries (Supplemental Figure S6, A and B).

These model results can be understood from an energetic perspective. The minimum-energy principle mandates that the CSs are driven to either the attractive energy well (i.e., clustering) or the repulsive energy well (i.e., wide separation). Note that the repulsive energy well in our model is deeper than the attractive well (Supplemental Table S1), which is necessary for favoring bipolarity over monopolarity in normal cells with two CSs (Supplemental Figure S3). Hence, in principle, the total energy of the system is minimized and the most stable state is achieved if all CSs can be widely separated from each other. The limited space in a cell, however, may not allow such a full separation to happen (in terms of energy, full separation incurs a big penalty from the inward radial potential energy). In this case, CS clustering offers the next best solution, which combines the energetically optimal wide separation between clusters of CSs with the slightly higher energy in the attractive energy well for CSs within clusters. Overall, the total energy is minimized when the CSs form as many sufficiently distanced clusters as possible, given the space inside a cell. Bearing this general principle in mind, we can examine the effect of cell geometry. Compared with rounded cells, a severely flat cell has a larger equator (in the central *x*–*y* plane) in our model cell (Figure 5C, gray lines and circles). As shown below, the CSs tend to localize close to the equator (Figure 6). With the large space around the equator in a flat cell, the CSs can comfortably stay in the repulsive energy wells, while being scattered in multiple loci along the equator (Figure 5C, bottom row). In rounder cells, however, as the equator shrinks, the CSs cannot be separated far enough to stay low in the repulsive energy wells, unless they form only two clusters with the small price of raising the inter-CS energy slightly for the clustered CSs (Figure 5C, top row). In summary, the large equators in severely flat cells make multiple CS clusters energetically more favorable than two CS clusters, while the opposite is true in rounded cells (Figure 5C, sum of inter-CS energies).

Nevertheless, the cell does not need to be perfectly round to effectively cluster its extra CSs: the fractions of bipolar spindles and stable bipolar spindles are comparable between the perfectly round geometry and the slightly flat, default cell geometry (Figures 4, B and C, and 5A; Supplemental Figure S6, A and B). Importantly, the aforementioned findings are consistent with experimental observations that suppression of cell rounding beyond a critical threshold, such as that caused by physical confinement, can cause splitting of the spindle poles and multipolar division, even in cells with only two CSs (Tse *et al.*, 2012; Lancaster *et al.*, 2013;

Taubenberger *et al.*, 2020). Our model hence provides mechanistic insights into these intriguing observations.

Furthermore, our model predicts that flattening a cell can help orient the spindle (Figure 6). We plotted histograms of the altitude angles of the spindle poles at the end of the simulations (Figure 6A). In a perfectly round cell, the distribution of the angles matches the theoretical probability density function for a homogeneous distribution of the CSs around the cell surface (Figure 6B; Eq. S10 in Supporting Materials and Methods). In slightly flat and severely flat cells, compared with their respective theoretical homogeneous distributions, the spindle pole angles are dramatically concentrated around 0°, which is around the equator of the cell (Figure 6, C and D; Eq. S10 in Supporting Materials and Methods). This result can be understood with the same line of reasoning as mentioned previously. The short axis of the cell is not long enough to accommodate the repulsive energy well between CSs; hence, the CSs are driven toward the more spacious equator in the *x*–*y* plane. Of particular note, the slight flatness in the default geometry is sufficient to orient the spindle to an extent that is indistinguishable from a severely flat cell (Figure 6, C and D). Combined with the finding that the default geometry facilitates bipolar spindle formation as effectively as a perfectly round cell (Figures 4 and 5), the slightly flat default geometry can therefore fulfill two functions simultaneously: promoting bipolar spindle formation and aligning the spindle axis parallel to the equatorial plane of the cell. This may explain why mitotic cells round up but typically not to the point of becoming perfect spheres.

Smaller cell size promotes bipolar CS clustering

We next examined the effect of cell size by varying the cell volume in our model. Because cell size is often coupled with cell geometry (Cadart *et al.*, 2014; Bloomfield *et al.*, 2021), we used the model to investigate how cell size and aspect ratio jointly affect CS clustering in a cell with four CSs. The model predicts that a larger cell volume promotes multipolarity, whereas a smaller cell volume facilitates bipolar CS clustering (Figure 7A). The reason for these results is the same as those given in the previous section, that is, a larger space makes CS separation energetically more favorable. In smaller cells, multiple CS clusters cannot be separated far enough to rest in the repulsive energy well (Figure 1C) and hence the CSs have to aggregate in two clusters to achieve minimum total energy. If the cell volume becomes so small that even two clusters cannot be sufficiently distanced from each other, then all CSs would collapse into a monopolar spindle at a significant probability (Figure 7A, bottom left region), and bipolar spindles, even if formed, are less stable (Supplemental Figure S8, A and B, bottom left region). Finally, similar to the previous results (Figure 5), a smaller aspect ratio promotes CS clustering and vice versa (Figure 7A).

To test these model predictions, we took advantage of various tetraploid (4N) DLD-1 cell clones with significantly different cell sizes (Supplemental Figure S7A). The clones of large cells (L clones) also exhibited significantly larger cell aspect ratio in mitosis than the clones of small cells (S clones) (Supplemental Figure S7B). If we assume that only the cell size and aspect ratio differed among the 4N clones, whereas the other factors were largely consistent due to their nearly identical genetic background, then the model would predict a higher rate of bipolar CS clustering in the small 4N clones compared with the large 4N clones (Figure 7A, right). Indeed, despite the fraction of mitotic cells with extra CSs being similar in all 4N clones (Supplemental Figure S7C), there were substantially higher fractions of cells with multipolar spindles in the large 4N clones than the small 4N clones (Supplemental Figure S7D). This suggests that compared with large cells, small 4N cells with extra CSs were more efficient at clustering their CSs and forming bipolar spindles (Figure 7B; Supplemental Figure S7E), which is consistent with our model prediction.

Together, we found that cell shape and cell size both affect the spindle state, and bipolar CS clustering is promoted in rounder and smaller cells.

Exclusion of CSs from the cell center promotes stable bipolar spindle

CSs are typically excluded from the center of a mitotic cell: in prophase, they are located outside the nucleus, and after nuclear envelope breakdown, they continue to be excluded from the dense chromosome mass that occupies the center of the cell, as well as getting pulled toward the cell cortex by cortical dynein (Wittmann *et al.*, 2001; Moore and Cooper, 2010). In our model, exclusion of CSs from the center of the cell is characterized by the radial potential energy (Eq. 4), particularly the outward half of the potential energy (the inward radial force simply represents the hard boundary of the cell). Here, we used the model to explore whether exclusion of CSs from the cell center might play any functional role in bipolar spindle formation.

Our model results indicate that the outward force does not significantly affect the distribution of spindle states at the end of the 2-h simulations (Figure 8A; Supplemental Figure S9, A and D). However, a sufficient level of outward force is necessary for the stability of bipolar spindles (Figure 8, B and C; Supplemental Figure S9, B, C, E, and F). This model result can be understood in the following way: stability of a bipolar spindle with extra CSs depends on how easily a CS can escape the energy wells caused by intracluster attraction and intercluster repulsion. If the CS can escape easily, then the spindle is unstable. Vice versa, difficulty in escaping stabilizes the spindle. Furthermore, the escape is mediated by random fluctuations—both intrinsic fluctuations of the CS itself and fluctuations of inter-CS forces. In a bipolar spindle, these random fluctuations cause a CS to move either perpendicular or parallel to the spindle axis (Figure 8D, top left). The outward radial force, however, acts as a rectifier that inhibits CS movements parallel to the spindle axis. Consequently, fluctuations in the distance between the two CS clusters are suppressed (Figure 8D, red path inhibited by outward radial force). In other words, by keeping CSs near the cell membrane, the outward radial force prohibits the CS to escape from the energy well caused by intercluster repulsion; this helps sustain the bipolar spindle (Supplemental Movie S2). Without the outward force, the CS can easily move parallel to the spindle axis toward the center of the cell, which facilitates the transition into a transient multipolar state (Supplemental Movie S3) or a different bipolar spindle configuration (i.e., bipolarity with different sets of CSs clustered) (Supplemental Movie S4). Although the spindle may still end up bipolar, frequent CS translocations can cause merotelic kinetochore-MT attachments, a major cause of chromosome missegregation and aneuploidy (Silkworth and Cimini, 2012). In summary, the outward radial force stabilizes the bipolar spindle through inhibiting random translocation of CSs across the interior of the cell.

Cells with more CSs are less effective in bipolar CS clustering

Finally, we investigated how bipolar CS clustering depends on the number of CSs in the cell. The model predicts that cells with more CSs are less effective at forming a bipolar spindle (Figure 9), as well as at maintaining a stable bipolar spindle (Supplemental Figure S10). This is predicted because more CSs provide more metastable multipolar spindle configurations that compete with the bipolar configurations. (The spindle configuration refers to the specific

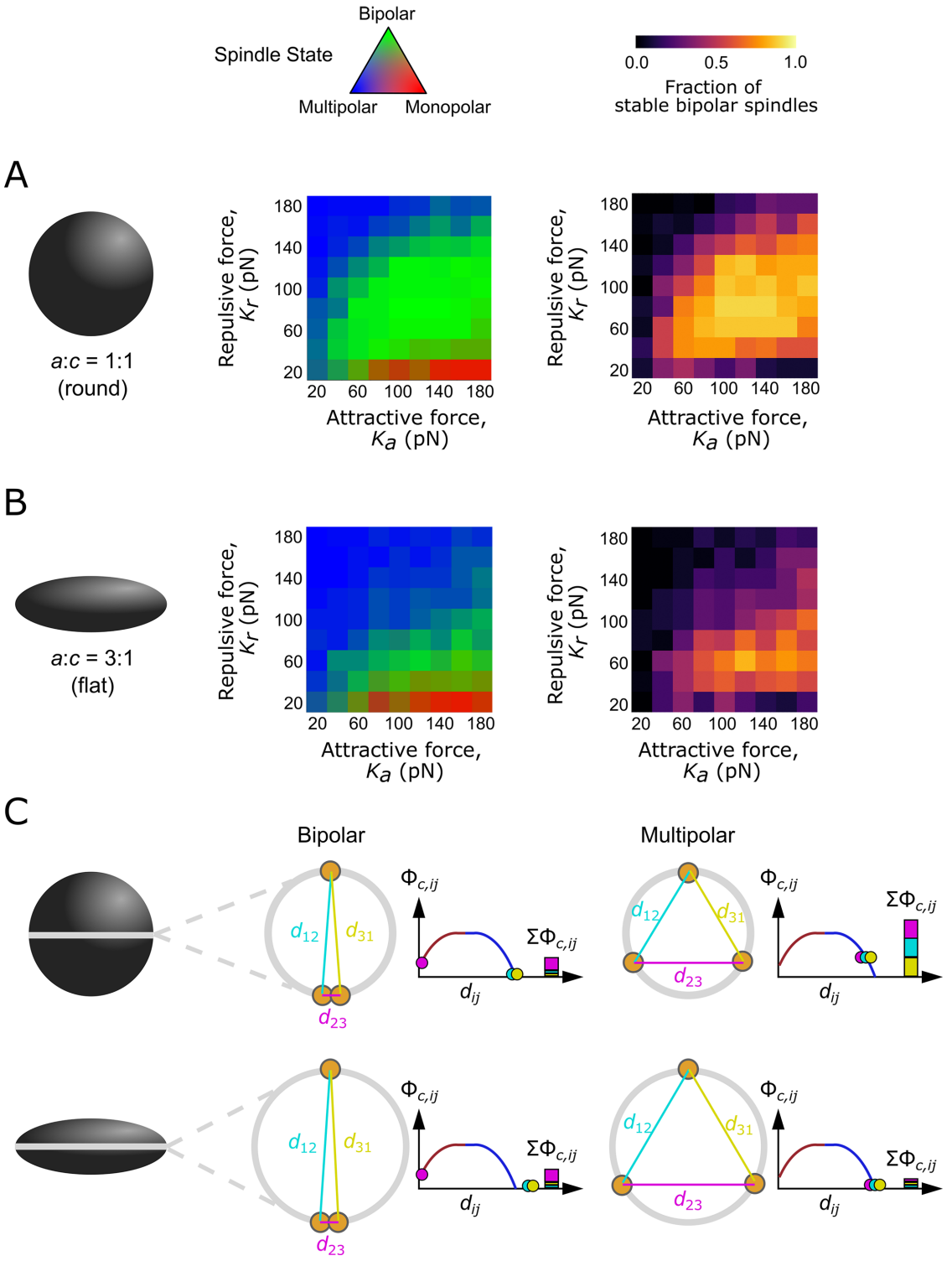

FIGURE 5: Effects of cell geometry on spindle formation with four CSs. (A and B) Model predicted fractions of three spindle states (middle column, triangular color map on top) and stable bipolar spindles (right column, color bar on top) in a perfectly round cell (small aspect ratio) (A) and in a severely flat cell (large aspect ratio) (B). The aspect ratio refers to the ratio between the length of the *x*-/*y*-axis (*a*) and that of the *z*-axis (*c*) of the radial equilibrium surface (and the cell); the *x*- and *y*-axes assume the same length in all cells. Cells with different aspect ratios assume equal volume within their radial equilibrium surfaces. Predictions were made for varied inter-CS attractive and repulsive force intensities, like in Figure 4, B and C. Thirty 2-h stochastic simulations were performed for each parameter set. (C) Illustration of why flat cell geometry favors the multipolar state using examples with three CSs in the cell. Gray lines and circles: equator (in the central *x*–*y* plane) in the model cell. Yellow solid circles: CSs. Colored dots on energy profile illustrate the inter-CS distances (color coded the same way for edges connecting yellow circles in the cartoon diagram) and corresponding inter-CS energies between each pair of CSs. Stacked colored bars illustrate summing of inter-CS energies in each case.

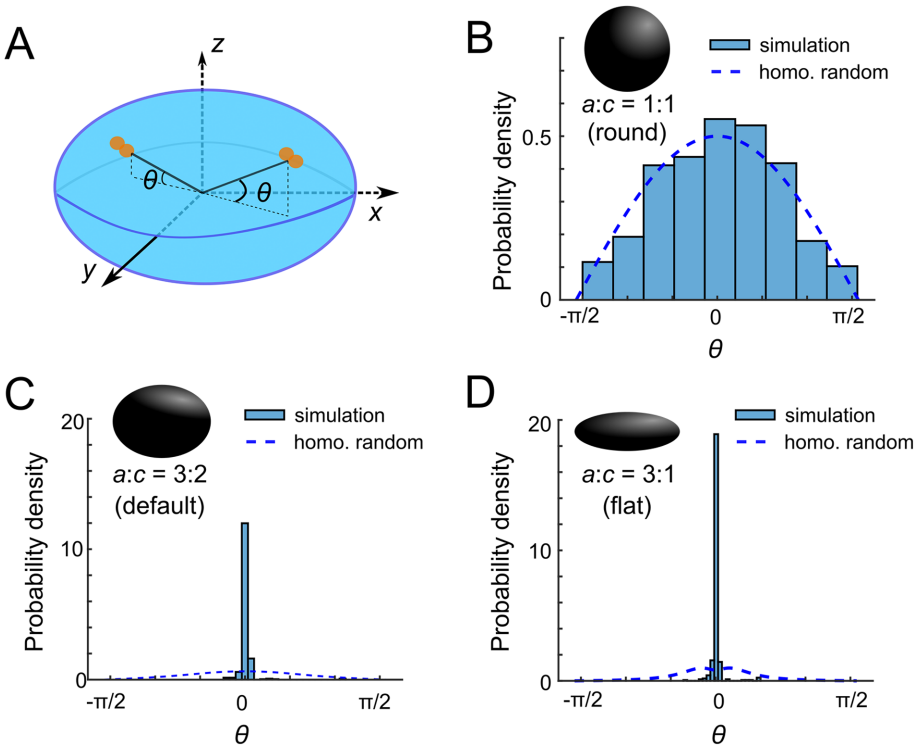

FIGURE 6: Flatness of a cell helps orient the spindle along the long axis of the cell. (A) The spindle orientation is quantified by the altitude angle θ of each spindle pole with respect to the equator in the x–y plane. This is where the two equal, long axes lie. (B, C, and D) Distribution of the altitude angle of spindle poles with a perfectly round geometry (B), the default, slightly flat geometry (C), and a severely flat geometry (D). Dashed curves: theoretical probability density of spindle pole angles if the poles are homogeneously distributed on the radial equilibrium surface (see derivation in Supporting Materials and Methods). Bars: histograms of 200 simulated spindle pole angles in each case.

arrangement of CSs in a particular spindle state.) In thermodynamic terms, this raises the entropy of the ensemble multipolar state, making it energetically more favorable. A more intuitive way to understand it is as follows: as the number of CSs in a clustered spindle pole increases, it is more likely that one or more CSs randomly escape from a CS cluster to reach another multipolar configuration.

DISCUSSION

Formation of a bipolar spindle is necessary for passing on a correct set of chromosomes to the daughter cells and is one of the most conserved and prominent cellular events in mitosis. In this study, we investigated how bipolar spindle formation can robustly take place when the cell is challenged by perturbations to its CSs, which organize the poles of the mitotic spindle. We specifically constructed an energy-based model to characterize the forces driving the movements of CSs during spindle formation. The model allowed us to identify important biophysical factors that facilitate the cell to both recover a bipolar spindle from monopolarity (in the case of normal two CSs) and cluster extra CSs into two poles (in the case of extra CSs).

Our model brings novel explanation to experimental phenomena

Findings from our model explain a wide array of experimental phenomena and reveal important design principles behind the molecular mechanism of spindle assembly. First, we found that temporal fluctuation in the inter-CS force with proper intensity and relaxation timescale aids bipolar spindle formation under both types of perturbations (Figure 3; Supplemental Figures S5 and S11). Notably, the predicted optimal relaxation timescale for the force fluctuation, approximately tens of second, matches the timescales associated with MT instability and binding/unbinding of MT-associated motors (Verde *et al.*, 1992; Belmont and Mitchison, 1996; Valentine *et al.*, 2006; Gardner *et al.*, 2011; Kunwar *et al.*, 2011; Norris *et al.*, 2018; Reinemann *et al.*, 2018), which are major sources of the force fluctuation. Recent studies, indeed, indicated the importance of MT instability and dynamic motor-MT attachment for CS separation and bipolar spindle assembly (Mitchison *et al.*, 2005; Lamson *et al.*, 2019).

Second, we found the balance between inter-CS attraction and repulsion to be important for establishing bipolar spindles (Figure 4). Consistent with our model prediction, simultaneous inhibition of motors that generate attraction and repulsion between CSs results in bipolar spindle formation, although inhibition of single motors results in abnormal spindle assembly (Gaglio *et al.*, 1996; Saunders *et al.*, 1997; Mountain *et al.*, 1999; Tanenbaum *et al.*, 2008; van Heesbeen *et al.*, 2014; Neahring *et al.*, 2021).

Third, the model predicted that cell rounding facilitates CS clustering and bipolar spindle formation (Figure 5). Indeed, mitotic cell rounding is a universal property of animal cell division and plays an important role in facilitating successful cell division (Taubenberger *et al.*, 2020). Disruption of cell rounding, for instance, by physical confinement, causes severe deformation of the mitotic spindle, particularly spindle pole splitting and subsequent multipolar division, even in normal cells with two CSs (Tse *et al.*, 2012; Lancaster *et al.*, 2013). Although CSs act as major MT-organizing centers in the cell, spindle MTs can assemble via CS-independent pathways; therefore, even normal mitotic cells with two CSs can suffer from multipolarity under extreme perturbations. These experimental phenomena can hence be compared with our model results about cell rounding for cells with extra CSs (Figure 5). Contrasting the previous theory that flattened cells do not provide enough room for spindle formation (Taubenberger *et al.*, 2020), our model suggests that flattened cells have a larger equator, which can energetically

CSs tend to be localized around the edge of the equator in our model results. In a round cell, the equator is small, which prevents inter-CS distances in the multipolar state to all reach the repulsive energy well (top right diagram). Consequently, the total energy is lower in the bipolar state. In contrast to the round cell, a flat cell with the same cell volume has a larger equator; in this large equator, the distances between multiple spindle poles are all long enough to reach the repulsive energy well (bottom right diagram). Consequently, the total energy is lower in the multipolar state.

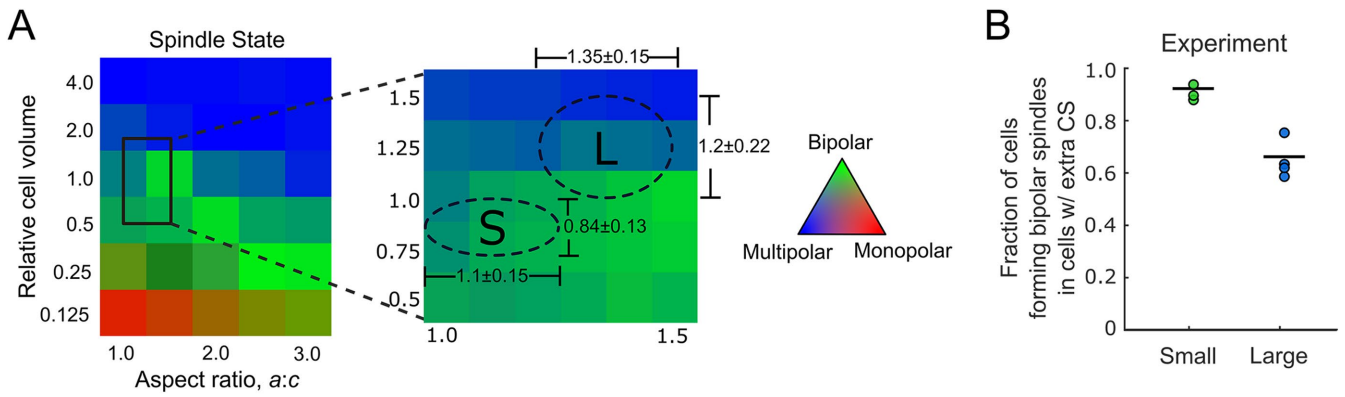

FIGURE 7: Cell size and aspect ratio both affect spindle state. (A) Model predicted fractions of three spindle states with varied cell volume and aspect ratio in cells with four CSs (color coded according to the color triangle on the right). Thirty 2-h stochastic simulations were performed for each parameter set. The plot on the right shows simulated results with denser data points in a smaller parameter range covering the experimentally observed relative cell volumes (0.5–1.5) and aspect ratios (1.0–1.5) in tetraploid DLD-1 cell clones (Supplemental Figure S7). Relative cell volume in the model was calculated by dividing the volume enclosed by the radial equilibrium surface by that for the default parameter set (Supplemental Table S1). The experimental relative cell volume was calculated by dividing with the measured cell volume by 3100 μm^3 (approximate mean volume of all cells). Dashed circles labeled with "S" and "L" mark the range defined by mean relative volume ± SEM and mean aspect ratios ± SEM observed in clones of small cells and large cells, respectively (Supplemental Figure S7). (B) Experimentally measured fraction of cells forming bipolar spindles in the cells with extra CSs in small and large tetraploid DLD-1 clones. Lines: mean fractions. Dots: values in experimental replicates (from Supplemental Figure S7E).

favor multiple spindle poles (Figure 5C). Moreover, a slight flatness can help orient the spindle (Figure 6) without affecting bipolar spindle formation (Figure 4). Indeed, mitotic spindles are observed to align with the long axis of the cell (O'Connell and Wang, 2000; Strauss *et al.*, 2006; Minc *et al.*, 2011; Xiong *et al.*, 2014) (which corresponds to the *x*–*y* equatorial plane in our model as the cell assumes the shape of an oblate spheroid). Previous models suggest that the alignment is mediated by the cortical force exerted by dynein on the astral MTs (Minc *et al.*, 2011; Li and Jiang, 2018; Li *et al.*, 2019). Here, our model provides an additional explanation based on the inter-CS energies.

Fourth, our model predicted that smaller and rounder cells tend to be more effective in bipolar CS clustering whereas larger and flatter cells are more prone to forming multipolar spindles. This prediction was verified by our experiments on tetraploid cell clones of different cell sizes (Figure 7). It is important to note that in very large cells such as oocytes, the chromosomes and MT network are surrounded by an actin network, and proper chromosome attachment and alignment are promoted by the actin network (Lenart *et al.*, 2005; Mori *et al.*, 2011; Uraji *et al.*, 2018; Booth *et al.*, 2019); it is possible that the actin network may also facilitate bipolar spindle formation through confining the spindle components to a much smaller physical space than the whole cell.

Fifth, we found that the outward radial force helps stabilize the bipolar spindle and prevent transient CS translocation that could cause merotelic kinetochore-MT attachments and chromosome missegregation (Figure 8; Supplemental Figure S9). This finding points out one functional role of exclusion of CSs from the cell center, especially by active mechanisms such as pulling by cortical dynein. This novel role contrasts with the established function of cortical dynein and cortical force in regulating spindle assembly, spindle positioning, and CS clustering in relation to the extracellular environment (Basto *et al.*, 2008; Kiyomitsu and Cheeseman, 2012; Knouse *et al.*, 2018; Mercadante *et al.*, 2023).

Finally, our model predicts that increasing the number of extra CSs in a cell impedes bipolar spindle formation (Figure 9). This could explain the rarity of cells with more than four CSs in cell populations with elevated frequency of supernumerary CSs (Okuda *et al.*, 2000; Fisk and Winey, 2001; Tarapore *et al.*, 2002; Denu *et al.*, 2016; Baudoin *et al.*, 2020)—these cells would have difficulty forming a bipolar spindle and would produce unviable cells as a result of multipolar division and severe chromosome segregation errors.

Our model suggests a unified thermodynamic perspective to understand bipolar spindle formation

Our model provides a novel and unified thermodynamic perspective to understand the effects of biophysical factors on robust bipolar spindle formation. This thermodynamic understanding can be illustrated by how the free-energy landscape of spindle state depends on each biophysical factor (Figure 10). Note that a particular factor may affect the free energies associated with the monopolar, bipolar, and multipolar states by changing their enthalpy and/or entropy (free energy = enthalpy − temperature × entropy) (Figure 10A). Generally speaking, enthalpy is associated with the depth of the potential energy wells (deeper energy well corresponds to lower enthalpy), whereas entropy, as a measure of disorder, is associated with the number of "microconfigurations" in a spindle state (i.e., combination of specific locations of each CS). When a state assumes a lower free energy with respect to the other states, it becomes energetically more favorable and the cell is more likely to approach such a state of low free energy. For our default parameter set, the bipolar state assumes the lowest free energy and is most favorable.

Now let us consider the effect of each biophysical factor. Increasing the inter-CS attraction deepens the attractive well of the inter-CS energy, which strongly decreases the enthalpy and free energy of the monopolar state relative to the other two states and thus promotes the monopolar state (Figure 10, B-i). Increasing inter-CS repulsion does exactly the opposite and promotes the multipolar state (Figure 10, B-ii). Increasing the cell size or aspect ratio enlarges the physical space in which the CSs tend to lie in (i.e., the equator), which not only avoids the enthalpic penalty of CS scattering that

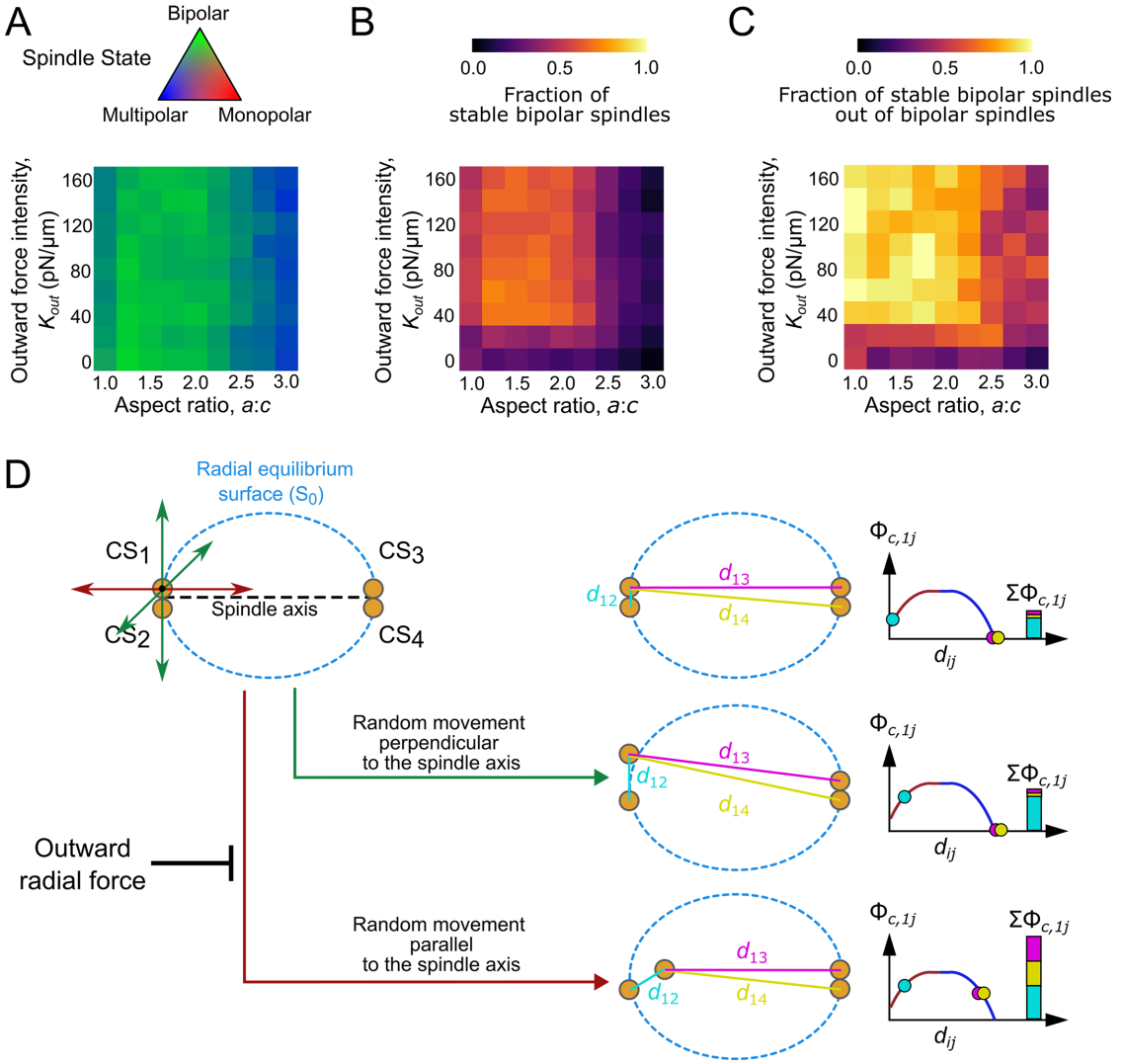

FIGURE 8: Outward radial force promotes stable bipolar spindles. (A) Model predicted fractions of three spindle states with varied outward radial force intensity and cell aspect ratio (color coded according to the color triangle on the top). (B) Model predicted fraction of stable bipolar spindles out of all simulations. (C) Model predicted fraction of stable bipolar spindles out of bipolar spindles. Thirty 2-h stochastic simulations were performed for each parameter set. (D) Illustration of why the outward radial force promotes stable bipolar spindle. Random CS movements parallel to the spindle axis (red path) significantly affect inter-CS energies both within and between clusters, whereas those perpendicular to the spindle axis (green path) only significantly affect the energies within clusters. Therefore, the parallel fluctuation is more effective in helping the system cross the energy barrier and reach another spindle configuration, which disrupts stability of the spindle. Because the outward force inhibits CS movements parallel to the spindle axis (red path inhibited), it stabilizes the bipolar spindle.

happens to small spaces (Figure 5C) but also increases the entropy of the multipolar state with respect to the other two states (as there are more possible multipolar configurations than monopolar and bipolar ones). Overall, the free energy of the multipolar state is lower than the other two states when the cell size or cell aspect ratio is large (Figure 10, B-iii and iv). Increasing the CS number lowers the enthalpy of all three spindle states, as each CS interacts with more CSs through attraction or repulsion. But a larger CS number specifically introduces more combinations of CS locations in the multipolar state and hence increases the entropy of the state. Therefore, the multipolar state achieves a lower free energy than the other two tates (Figure 10, B-v). Increasing the inter-CS force fluctuation does not change the relative free energy of the three spindle states but

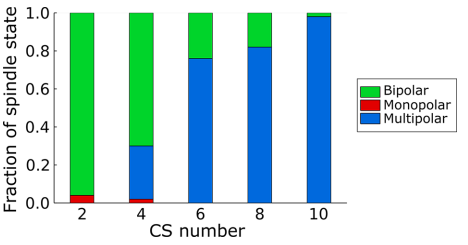

FIGURE 9: Predicted fractions of bipolar and multipolar spindles with various CS numbers. Fifty 2-h stochastic simulations were performed for each CS number. CSs were initially randomly scattered in each simulation.

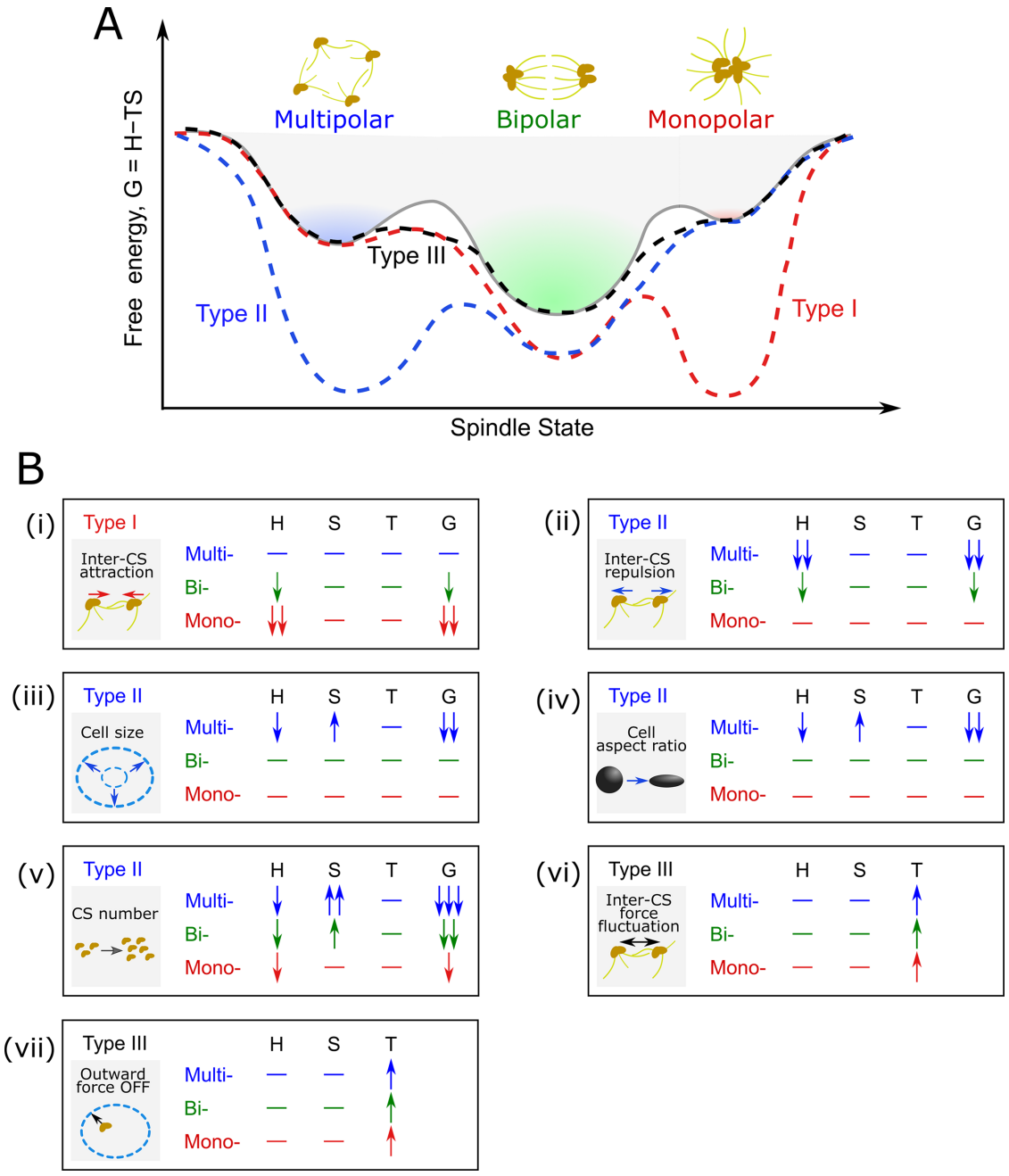

FIGURE 10: Thermodynamic view of the effects of each biophysical factor. (A) Three types of effects on the free energy of the multipolar, bipolar, and monopolar states. G = free energy, H = enthalpy, T = temperature, and S = entropy. The solid curve with gray background represents the free-energy landscape of the default parameter set. The colored dashed lines represent three types of possible impacts by the biophysical factors. Note that the dashed lines illustrate the relative, rather than absolute, free energy of the three spindle states, as only the relative free energy matters for the thermodynamic outcome. (B) Effects of stronger inter-CS attraction (i), stronger inter-CS repulsion (ii), larger cell size (iii), larger cell aspect ratio (iv), larger CS number (v), stronger inter-CS force fluctuation (vi), and elimination of outward radial force (vii), respectively, on the free energy of the spindle states. Labeled types correspond to the types in (A).

rather imposes an effect similar to increasing the temperature of the system or lowering the energy barriers between each state (Figure 10, B-vi). This allows the system to escape more readily from the monopolar state and reach the bipolar state; however, too much fluctuation would make the bipolar spindle unstable. Finally, shutting off the outward radial force has an analogous effect to increasing the inter-CS force fluctuation, because the outward radial force rectifies the random fluctuations along the spindle axis (Figure 8D). Hence, this is also analogous to increasing the temperature of the system or lowering the energy barriers between states (Figure 10, B-vii). Altogether, bipolar spindle formation can be regarded as a result of balanced energetic control by these biophysical factors.

Our model provides a succinct theoretical framework for spindle assembly

Compared with agent-based models that have been widely used in the study of spindle assembly, formulating our model with simple effective potential energies provided several advantages. First, the

simple energetic model can be simulated with a much lower computational cost. This is especially advantageous for stochastic models, for which small time steps and multiple random repeats are necessary. The low computational cost allows us to comprehensively explore the model's behavior over its parameter space. Second, the simple model allows us to distill the fundamental principles underlying bipolar spindle formation more easily. Although agent-based models, when equipped with well-tuned parameters, can provide more accurate and detailed predictions, it is often difficult to understand why exactly the predictions emerge as the model is highly complex. When this happens, the model fails to bring insight into the biological system. In contrast, our simple model provides a unified base to explain various predictions and thus valuable insights into the corresponding experimental phenomena. Although simplified, our model's ability to account for numerous experimental phenomena in spindle assembly suggests that the majority of the intricate process of spindle assembly can be captured by these succinct fundamental principles. For example, the complex direct and indirect mechanical forces between CSs must be attractive over short distances and repulsive over long distances, plus additional fluctuations in the forces. These demonstrate crucial design principles of spindle self-assembly regardless of which molecules actually carry out the process.

Comparison with previous models

A similar energy-based modeling approach was adopted by Chatterjee *et al.* (2020) to model CS clustering. In Chatterjee *et al.* (2020), the authors used Monte Carlo method to estimate the probability of reaching different configurations based on their energies, without considering the actual dynamics. This is similar to the thermodynamic principle that governs the behavior of our model. Unlike our model, however, Chatterjee's model resolves individual chromosomes, which play important roles in CS clustering, such as sterically blocking CS clustering (Goupil *et al.*, 2020) or generating torque to promote CS clustering (Miles *et al.*, 2022). But it should be noted that these chromosome-mediated effects are all combined in our model into the inter-CS and radial potential energies. Particularly, the steric blockage by chromosomes (Goupil *et al.*, 2020) likely provides part of the inter-CS repulsion. Stabilizing MTs, as that tested in Goupil *et al.* (2020), likely shrinks the spatial range of inter-CS repulsion, as longer MTs could allow the CSs to bypass the chromosome-mediated blockage, form attractive interactions between each other, and hence cancel out the repulsive interactions. In this case, our model would also predict promotion of bipolar spindle formation (Supplemental Figure S6A), like that observed in the model and experiments of Goupil *et al.* (2020). Furthermore, the torque that rotates the chromosomes with respect to the CSs (Miles *et al.*, 2022) provides part of the inter-CS attraction if two CSs are connected to the same kinetochore of the chromosome, or inter-CS repulsion if they are connected to the sister kinetochores. More interestingly, when we assessed the total effective energy associated with any given target CS (while all the other components are fixed in space), the spatial pattern of this energy is qualitatively similar between our model and Chatterjee's model for typical spatial distributions of the chromosomes found at different stages of prometaphase (Supplemental Figures S12–S14). Not surprisingly, both our study and the study by Chatterjee *et al.* (2020) identified balance between inter-CS attraction and repulsion as a crucial factor for achieving bipolar CS clustering.

However, a critical addition of our model compared with Chatterjee's model is the dynamics of the process, as the spindle must become bipolar within a biologically relevant time and stay bipolar for sufficiently long. With explicit stochastic simulation of CS movements, we were able to explore how the spindle achieves bipolarity with reasonable timing and stability. In particular, our study has pointed out the importance of inter-CS force fluctuation in enabling proper timescale of bipolar spindle formation and maintenance, and provided insights into how CSs strike a balance between separation and clustering to form two spindle poles.

Note that while Chatterjee's model reports the probabilities of each spindle state based on an energy equilibrium, our model reports the probabilities away from equilibrium. Equilibrium, as that assumed in Chatterjee's work, implies fast transition among different spindle states, which essentially corresponds to an unstable spindle. In contrast, in the nominal case of our model the state transitions happen on a comparable timescale as mitotic duration. This allows transition into the lowest energy state to take place within the timescale of mitotic duration, but there is usually insufficient time to transition out of it. Because the spinßßßßßßdle cannot make state transitions multiple times during mitosis, the system is essentially operating away from equilibrium. Of note, this intermediate transition time is necessary to rescue both monopolar and multipolar anomalies in our model. This is because the inter-CS energy of clustered CSs cannot be too different from that of separated CSs; otherwise, the system is unavoidably biased toward either the monopolar or the multipolar spindle. Given the limited energy difference between different spindle states, the requirement for quick escape from the monopolar and multipolar states conflicts with the requirement for prolonged persistence in the bipolar state. This conflict can be resolved only through the differential transition times explained previously. When the system is operating away from equilibrium, the probabilities of arriving at a state can be very different from those in an equilibrium case. It is therefore not surprising to find some contrasting predictions between the two models, such as the dependence of spindle state on cell size.

Caveats and future work

Certain assumptions in our current model may be oversimplified and can be modified in future work. First, our current model focuses on CS dynamics, while lumping the dynamics of all other subcellular organelles, such as the chromosomes, MT network, and molecular motors, into the potential energies acting on the CSs. In principle, such simplifications approximate the true dynamics well if the dynamics of the lumped components is much faster than the CS dynamics that is explicitly resolved in the model, and their configurations are roughly reversible as the CSs return to earlier positions. This condition, however, may not be true for all the lumped components. For future work, we will refine the model with explicit consideration of additional subcellular components and investigate to what extent these approximations are good. Of course, future experiments will also provide more information in this regard.

Second, the study is built upon the premise that rescues from monopolar and multipolar spindles are mediated by the same molecular machinery as the unperturbed normal bipolar mitosis. Hence, the two cases were modeled as two different initial conditions with the same parameter values. We would like to point out that this is true in certain scenarios. In some unperturbed cells, for instance, CSs do not separate before nuclear envelope breakdown (Rattner and Berns, 1976; Aubin *et al.*, 1980; Waters *et al.*, 1993; Whitehead *et al.*, 1996; Rosenblatt *et al.*, 2004; Toso *et al.*, 2009) and normal spindle assembly in this case is technically equivalent to a rescue from the monopolar state. Moreover, cells that acquire four CSs through whole genome doubling have their MT abundance doubled as well. In the model, correspondingly, the overall inter-CS potential energies and forces scale with CS number when the parameters stay unchanged. Nevertheless, some defective scenarios may call for different parameter values. For example, if MT abundance

does not change with CS number, then the parameters for inter-CS forces may need to scale inversely with CS number. It would be interesting for future experimental studies to compare the occurrences of various spindle states among CS abnormalities that arise from different causes and check the data against the model predictions based on different parameter sets.

Third, the effective potential energies are assumed to be fixed during mitosis. In reality, MT dynamics are affected by intracellular signals. For instance, rapid degradation of cyclin B in late mitosis stabilizes the MTs connected to the kinetochores (Vazquez-Novelle *et al.*, 2014), which constitute a significant fraction of MTs in late mitosis. As a result, inter-CS force fluctuation could be reduced in late mitosis; according to our model, reduction of force fluctuation would stabilize the spindle. Meanwhile, destruction of cyclin B is promoted by bioriented attachment of the kinetochores to the MT spindle (Musacchio and Salmon, 2007). Therefore, control of MT dynamics by cyclin B provides an extra screening mechanism that favors stable bipolar spindles. To better capture the changes in spindle dynamics at distinct mitotic stages, in the future we will expand the model by accounting for the dependence of the potential energies on key intracellular signals as experiments suggest.

Finally, when exploring the effect of cell size/shape, we assumed that the potential energies do not change with cell size/shape. This assumption is reasonable when comparing cells with close genetic background and cell type, such as the tetraploid cell clones reported in this work, which derived from the same parental diploid cells. However, when the difference in cell size/shape is due to different genetic background or distinct cell types (e.g., small somatic cells vs. large oocytes), the MT and motor dynamics may be modulated differently and hence the potential energies could change. For future work, it will be interesting to experimentally measure MT and motor dynamics in different cell types, derive the corresponding effective potential energies in our model based on the data, and test whether our model prediction on the effect of cell size/shape holds true across different cell types.

CONCLUSION

Overall, our model provides critical mechanistic insights into bipolar spindle formation and a useful framework for future modeling and experimental studies on this topic. Particularly, the principles behind robust bipolar spindle formation that we learned from the model can guide construction of more detailed and accurate models in the future. Combined with experimental investigations, the knowledge gained will enable translational applications such as innovative cancer therapies that target the CS clustering process.

ACKNOWLEDGMENTS

This work was supported by National Institutes of Health (NIH) Grant 1R35GM138370 (J.C.), National Science Foundation (NSF) Grant MCB-1517506 (D.C.), and NIH Grant 1R01GM140042 (D.C.). We acknowledge members of the Cimini and Chen labs for helpful discussions and feedback. We also thank Dr. Alexey Khodjakov (Wadsworth Center, New York State Department of Health, Albany, NY) for providing the pcDNA3-γTGFP (γ-tubulin/green fluorescent protein) plasmid.

REFERENCES

Aubin JE, Osborn M, Weber K (1980). Variations in the distribution and migration of centriole duplexes in mitotic PtK2 cells studied by immunofluorescence microscopy. J Cell Sci 43, 177–194.

Basto R, Brunk K, Vinadogrova T, Peel N, Franz A, Khodjakov A, Raff JW (2008). Centrosome amplification can initiate tumorigenesis in flies. Cell 133, 1032–1042.

Baudoin NC, Nicholson JM, Soto K, Martin O, Chen J, Cimini D (2020). Asymmetric clustering of centrosomes defines the early evolution of tetraploid cells. eLife 9, e54565.

Belmont LD, Mitchison TJ (1996). Identification of a protein that interacts with tubulin dimers and increases the catastrophe rate of microtubules. Cell 84, 623–631.

Blackwell R, Edelmaier C, Sweezy-Schindler O, Lamson A, Gergely ZR, O'Toole E, Crapo A, Hough LE, McIntosh JR, Glaser MA, Betterton MD (2017). Physical determinants of bipolar mitotic spindle assembly and stability in fission yeast. Sci Adv 3, e1601603.

Bloomfield M, Chen J, Cimini D (2021). Spindle architectural features must be considered along with cell size to explain the timing of mitotic checkpoint silencing. Front Physiol 11, 596263.

Booth AJR, Yue Z, Eykelenboom JK, Stiff T, Luxton GWG, Hochegger H, Tanaka TU (2019). Contractile acto-myosin network on nuclear envelope remnants positions human chromosomes for mitosis. eLife 8, e46902.

Burbank KS, Mitchison TJ, Fisher DS (2007). Slide-and-cluster models for spindle assembly. Curr Biol 17, 1373–1383.

Cadart C, Zlotek-Zlotkiewicz E, Le Berre M, Piel M, Matthews HK (2014). Exploring the function of cell shape and size during mitosis. Dev Cell 29, 159–169.

Cai S, Weaver LN, Ems-McClung SC, Walczak CE (2009). Kinesin-14 family proteins HSET/XCTK2 control spindle length by cross-linking and sliding microtubules. Mol Biol Cell 20, 1348–1359.

Chan JY (2011). A clinical overview of centrosome amplification in human cancers. Int J Biol Sci 7, 1122–1144.

Charnley M, Anderegg F, Holtackers R, Textor M, Meraldi P (2013). Effect of cell shape and dimensionality on spindle orientation and mitotic timing. PLoS One 8, e66918.

Chatterjee S, Sarkar A, Zhu J, Khodjakov A, Mogilner A, Paul R (2020). Mechanics of multicentrosomal clustering in bipolar mitotic spindles. Biophys J 119, 434–447.

Civelekoglu-Scholey G, He B, Shen M, Wan X, Roscioli E, Bowden B, Cimini D (2013). Dynamic bonds and polar ejection force distribution explain kinetochore oscillations in PtK1 cells. J Cell Biol 201, 577–593.

Civelekoglu-Scholey G, Sharp DJ, Mogilner A, Scholey JM (2006). Model of chromosome motility in Drosophila embryos: adaptation of a general mechanism for rapid mitosis. Biophys J 90, 3966–3982.

Cytrynbaum EN, Scholey JM, Mogilner A (2003). A force balance model of early spindle pole separation in Drosophila embryos. Biophys J 84, 757–769.

Denu RA, Zasadil LM, Kanugh C, Laffin J, Weaver BA, Burkard ME (2016). Centrosome amplification induces high grade features and is prognostic of worse outcomes in breast cancer. BMC Cancer 16, 47.

Edelmaier C, Lamson AR, Gergely ZR, Ansari S, Blackwell R, McIntosh JR, Glaser MA, Betterton MD (2020). Mechanisms of chromosome biorientation and bipolar spindle assembly analyzed by computational modeling. eLife 9, e48787.

Elting MW, Suresh P, Dumont S (2018). The spindle: integrating architecture and mechanics across scales. Trends Cell Biol 28, 896–910.

Ferenz NP, Paul R, Fagerstrom C, Mogilner A, Wadsworth P (2009). Dynein antagonizes eg5 by crosslinking and sliding antiparallel microtubules. Curr Biol 19, 1833–1838.

Fisk HA, Winey M (2001). The mouse Mps1p-like kinase regulates centrosome duplication. Cell 106, 95–104.

Gaglio T, Saredi A, Bingham JB, Hasbani MJ, Gill SR, Schroer TA, Compton DA (1996). Opposing motor activities are required for the organization of the mammalian mitotic spindle pole. J Cell Biol 135, 399–414.

Ganem NJ, Godinho SA, Pellman D (2009). A mechanism linking extra centrosomes to chromosomal instability. Nature 460, 278–282.

Gardner MK, Zanic M, Gell C, Bormuth V, Howard J (2011). Depolymerizing kinesins Kip3 and MCAK shape cellular microtubule architecture by differential control of catastrophe. Cell 147, 1092–1103.

Gergely F, Basto R (2008). Multiple centrosomes: together they stand, divided they fall. Genes Dev 22, 2291–2296.

Godinho SA, Pellman D (2014). Causes and consequences of centrosome abnormalities in cancer. Philos Trans R Soc Lond B Biol Sci 369, 20130467.

Goshima G, Nedelec F, Vale RD (2005). Mechanisms for focusing mitotic spindle poles by minus end-directed motor proteins. J Cell Biol 171, 229–240.

Goupil A, Nano M, Letort G, Gemble S, Edwards F, Goundiam O, Gogendeau D, Pennetier C, Basto R (2020). Chromosomes function as a barrier to mitotic spindle bipolarity in polyploid cells. J Cell Biol 219, e201908006.

Hepperla AJ, Willey PT, Coombes CE, Schuster BM, Gerami-Nejad M, McClellan M, Mukherjee S, Fox J, Winey M, Odde DJ, *et al.* (2014).

Minus-end-directed Kinesin-14 motors align antiparallel microtubules to control metaphase spindle length. Dev Cell 31, 61–72.
Hinchcliffe EH, Sluder G (2001). "It takes two to tango": understanding how centrosome duplication is regulated throughout the cell cycle. Genes Dev 15, 1167–1181.
Hoffmann I (2021). Centrosomes in mitotic spindle assembly and orientation. Curr Opin Struct Biol 66, 193–198.
Hu CK, Coughlin M, Field CM, Mitchison TJ (2008). Cell polarization during monopolar cytokinesis. J Cell Biol 181, 195–202.
Kapitein LC, Peterman EJ, Kwok BH, Kim JH, Kapoor TM, Schmidt CF (2005). The bipolar mitotic kinesin Eg5 moves on both microtubules that it crosslinks. Nature 435, 114–118.
Kapoor TM, Mayer TU, Coughlin ML, Mitchison TJ (2000). Probing spindle assembly mechanisms with monastrol, a small molecule inhibitor of the mitotic kinesin, Eg5. J Cell Biol 150, 975–988.
Khodjakov A, Copenagle L, Gordon MB, Compton DA, Kapoor TM (2003). Minus-end capture of preformed kinetochore fibers contributes to spindle morphogenesis. J Cell Biol 160, 671–683.
Kiyomitsu T, Cheeseman IM (2012). Chromosome- and spindle-pole-derived signals generate an intrinsic code for spindle position and orientation. Nat Cell Biol 14, 311–317.
Knouse KA, Lopez KE, Bachofner M, Amon A (2018). Chromosome segregation fidelity in epithelia requires tissue architecture. Cell 175, 200–211.e213.
Kozlowski C, Srayko M, Nedelec F (2007). Cortical microtubule contacts position the spindle in C. elegans embryos. Cell 129, 499–510.
Kramer A, Maier B, Bartek J (2011). Centrosome clustering and chromosomal (in)stability: a matter of life and death. Mol Oncol 5, 324–335.
Kunwar A, Tripathy SK, Xu J, Mattson MK, Anand P, Sigua R, Vershinin M, McKenney RJ, Yu CC, Mogilner A, Gross SP (2011). Mechanical stochastic tug-of-war models cannot explain bidirectional lipid-droplet transport. Proc Nat Acad Sci USA 108, 18960–18965.
Lampson MA, Renduchitala K, Khodjakov A, Kapoor TM (2004). Correcting improper chromosome-spindle attachments during cell division. Nat Cell Biol 6, 232–237.
Lamson AR, Edelmaier CJ, Glaser MA, Betterton MD (2019). Theory of cytoskeletal reorganization during cross-linker-mediated mitotic spindle assembly. Biophys J 116, 1719–1731.
Lancaster OM, Le Berre M, Dimitracopoulos A, Bonazzi D, Zlotek-Zlotkiewicz E, Picone R, Duke T, Piel M, Baum B (2013). Mitotic rounding alters cell geometry to ensure efficient bipolar spindle formation. Dev Cell 25, 270–283.
Landau LD, Lifshitz EM (1996). Statistical Physics, Vol. 5, 3rd ed., Oxford, England: Butterworth-Heinemann.
Lenart P, Bacher CP, Daigle N, Hand AR, Eils R, Terasaki M, Ellenberg J (2005). A contractile nuclear actin network drives chromosome congression in oocytes. Nature 436, 812–818.
Lens SMA, Medema RH (2019). Cytokinesis defects and cancer. Nat Rev Cancer 19, 32–45.
Li J, Cheng L, Jiang H (2019). Cell shape and intercellular adhesion regulate mitotic spindle orientation. Mol Biol Cell 30, 2458–2468.
Li J, Jiang H (2018). Regulating positioning and orientation of mitotic spindles via cell size and shape. Phys Rev E 97, 012407.
Liu J, Desai A, Onuchic JN, Hwa T (2007). A mechanobiochemical mechanism for monooriented chromosome oscillation in mitosis. Proc Nat Acad Sci USA 104, 16104–16109.
Liu J, Desai A, Onuchic JN, Hwa T (2008). An integrated mechanobiochemical feedback mechanism describes chromosome motility from prometaphase to anaphase in mitosis. Proc Nat Acad Sci USA 105, 13752–13757.
Magidson V, O'Connell CB, Loncarek J, Paul R, Mogilner A, Khodjakov A (2011). The spatial arrangement of chromosomes during prometaphase facilitates spindle assembly. Cell 146, 555–567.
Maiato H, Logarinho E (2014). Mitotic spindle multipolarity without centrosome amplification. Nat Cell Biol 16, 386–394.
Manneville JB, Etienne-Manneville S (2006). Positioning centrosomes and spindle poles: looking at the periphery to find the centre. Biol Cell 98, 557–565.
Marthiens V, Piel M, Basto R (2012). Never tear us apart—the importance of centrosome clustering. J Cell Sci 125, 3281–3292.
Mayer TU, Kapoor TM, Haggarty SJ, King RW, Schreiber SL, Mitchison TJ (1999). Small molecule inhibitor of mitotic spindle bipolarity identified in a phenotype-based screen. Science 286, 971–974.
Mercadante DL, Aaron WA, Olson SD, Manning AL (2023). Cortical dynein drives centrosome clustering in cells with centrosome amplification. Mol Biol Cell 34, ar63.
Miles CE, Zhu J, Mogilner A (2022). Mechanical torque promotes bipolarity of the mitotic spindle through multi-centrosomal clustering. Bull Math Biol 84, 29.
Milunovic-Jevtic A, Mooney P, Sulerud T, Bisht J, Gatlin JC (2016). Centrosomal clustering contributes to chromosomal instability and cancer. Curr Opin Biotechnol 40, 113–118.
Minc N, Burgess D, Chang F (2011). Influence of cell geometry on division-plane positioning. Cell 144, 414–426.
Mirabet V, Krupinski P, Hamant O, Meyerowitz EM, Jonsson H, Boudaoud A (2018). The self-organization of plant microtubules inside the cell volume yields their cortical localization, stable alignment, and sensitivity to external cues. PLoS Comput Biol 14, e1006011.
Mitchison TJ, Maddox P, Gaetz J, Groen A, Shirasu M, Desai A, Salmon ED, Kapoor TM (2005). Roles of polymerization dynamics, opposed motors, and a tensile element in governing the length of Xenopus extract meiotic spindles. Mol Biol Cell 16, 3064–3076.
Moore JK, Cooper JA (2010). Coordinating mitosis with cell polarity: molecular motors at the cell cortex. Semin Cell Dev Biol 21, 283–289.
Mori M, Monnier N, Daigle N, Bathe M, Ellenberg J, Lenart P (2011). Intracellular transport by an anchored homogeneously contracting F-actin meshwork. Curr Biol 21, 606–611.
Mountain V, Simerly C, Howard L, Ando A, Schatten G, Compton DA (1999). The kinesin-related protein, HSET, opposes the activity of Eg5 and cross-links microtubules in the mammalian mitotic spindle. J Cell Biol 147, 351–366.
Musacchio A, Salmon ED (2007). The spindle-assembly checkpoint in space and time. Nat Rev Mol Cell Biol 8, 379–393.
Neahring L, Cho NH, Dumont S (2021). Opposing motors provide mechanical and functional robustness in the human spindle. Dev Cell 56, 3006–3018.e5.
Nedelec F (2002). Computer simulations reveal motor properties generating stable antiparallel microtubule interactions. J Cell Biol 158, 1005–1015.
Norris SR, Jung S, Singh P, Strothman CE, Erwin AL, Ohi MD, Zanic M, Ohi R (2018). Microtubule minus-end aster organization is driven by processive HSET-tubulin clusters. Nat Commun 9, 2659.
O'Connell CB, Wang YL (2000). Mammalian spindle orientation and position respond to changes in cell shape in a dynein-dependent fashion. Mol Biol Cell 11, 1765–1774.
Ogden A, Rida PCG, Aneja R (2012). Let's huddle to prevent a muddle: centrosome declustering as an attractive anticancer strategy. Cell Death Differ 19, 1255–1267.
Okuda M, Horn HF, Tarapore P, Tokuyama Y, Smulian AG, Chan PK, Knudsen ES, Hofmann IA, Snyder JD, Bove KE, FukasawaK (2000). Nucleophosmin/B23 is a target of CDK2/cyclin E in centrosome duplication. Cell 103, 127–140.
Paul R, Wollman R, Silkworth WT, Nardi IK, Cimini D, Mogilner A (2009). Computer simulations predict that chromosome movements and rotations accelerate mitotic spindle assembly without compromising accuracy. Proc Nat Acad Sci USA 106, 15708–15713.
Prosser SL, Pelletier L (2017). Mitotic spindle assembly in animal cells: a fine balancing act. Nat Rev Mol Cell Biol 18, 187–201.
Quintyne NJ, Reing JE, Hoffelder DR, Gollin SM, Saunders WS (2005). Spindle multipolarity is prevented by centrosomal clustering. Science 307, 127–129.
Rattner JB, Berns MW (1976). Centriole behavior in early mitosis of rat kangaroo cells (PTK_2). Chromosoma 54, 387–395.
Reinemann DN, Norris SR, Ohi R, Lang MJ (2018). Processive kinesin-14 HSET exhibits directional flexibility depending on motor traffic. Curr Biol 28, 2356–2362. e5.
Rosenblatt J, Cramer LP, Baum B, McGee KM (2004). Myosin II-dependent cortical movement is required for centrosome separation and positioning during mitotic spindle assembly. Cell 117, 361–372.
Saunders W, Lengyel V, Hoyt MA (1997). Mitotic spindle function in Saccharomyces cerevisiae requires a balance between different types of kinesin-related motors. Mol Biol Cell 8, 1025–1033.
She ZY, Yang WX (2017). Molecular mechanisms of kinesin-14 motors in spindle assembly and chromosome segregation. J Cell Sci 130, 2097–2110.
Silkworth WT, Cimini D (2012). Transient defects of mitotic spindle geometry and chromosome segregation errors. Cell Div 7, 19.
Silkworth WT, Nardi IK, Scholl LM, Cimini D (2009). Multipolar spindle pole coalescence is a major source of kinetochore mis-attachment and chromosome mis-segregation in cancer cells. PLoS One 4, e6564.
Skoufias DA, DeBonis S, Saoudi Y, Lebeau L, Crevel I, Cross R, Wade RH, Hackney D, Kozielski F (2006). S-trityl-L-cysteine is a reversible, tight

binding inhibitor of the human kinesin Eg5 that specifically blocks mitotic progression. J Biol Chem 281, 17559–17569.
Som S, Chatterjee S, Paul R (2019). Mechanistic three-dimensional model to study centrosome positioning in the interphase cell. Phys Rev E 99, 012409.
Strauss B, Adams RJ, Papalopulu N (2006). A default mechanism of spindle orientation based on cell shape is sufficient to generate cell fate diversity in polarised Xenopus blastomeres. Development 133, 3883–3893.
Tanenbaum ME, Macurek L, Galjart N, Medema RH (2008). Dynein, Lis1 and CLIP-170 counteract Eg5-dependent centrosome separation during bipolar spindle assembly. EMBO J 27, 3235–3245.
Tanenbaum ME, Medema RH (2010). Mechanisms of centrosome separation and bipolar spindle assembly. Dev Cell 19, 797–806.
Tarapore P, Okuda M, Fukasawa K (2002). A mammalian in vitro centriole duplication system: evidence for involvement of CDK2/cyclin E and nucleophosmin/B23 in centrosome duplication. Cell Cycle 1, 75–81.
Taubenberger AV, Baum B, Matthews HK (2020). The mechanics of mitotic cell rounding. Front Cell Dev Biol 8, 687.
Tillement V, Remy MH, Raynaud-Messina B, Mazzolini L, Haren L, Merdes A (2009). Spindle assembly defects leading to the formation of a monopolar mitotic apparatus. Biol Cell 101, 1–11.
Toso A, Winter JR, Garrod AJ, Amaro AC, Meraldi P, McAinsh AD (2009). Kinetochore-generated pushing forces separate centrosomes during bipolar spindle assembly. J Cell Biol 184, 365–372.
Tse HT, Weaver WM, Di Carlo D (2012). Increased asymmetric and multi-daughter cell division in mechanically confined microenvironments. PLoS One 7, e38986.
Uraji J, Scheffler K, Schuh M (2018). Functions of actin in mouse oocytes at a glance. J Cell Sci 131, jcs218099.
Valentine MT, Fordyce PM, Krzysiak TC, Gilbert SP, Block SM (2006). Individual dimers of the mitotic kinesin motor Eg5 step processively and support substantial loads in vitro. Nat Cell Biol 8, 470–476.
van Heesbeen RGHP, Tanenbaum ME, Medema RH (2014). Balanced activity of three mitotic motors is required for bipolar spindle assembly and chromosome segregation. Cell Rep 8, 948–956.
Vazquez-Novelle MD, Sansregret L, Dick AE, Smith CA, McAinsh AD, Gerlich DW, Petronczki M (2014). Cdk1 inactivation terminates mitotic checkpoint surveillance and stabilizes kinetochore attachments in anaphase. Curr Biol 24, 638–645.
Verde F, Dogterom M, Stelzer E, Karsenti E, Leibler S (1992). Control of microtubule dynamics and length by cyclin A- and cyclin B-dependent kinases in Xenopus egg extracts. J Cell Biol 118, 1097–1108.
Vitre BD, Cleveland DW (2012). Centrosomes, chromosome instability (CIN) and aneuploidy. Curr Opin Cell Biol 24, 809–815.
Walczak CE, Heald R (2008). Mechanisms of mitotic spindle assembly and function. Int Rev Cytol 265, 111–158.
Waters JC, Cole RW, Rieder CL (1993). The force-producing mechanism for centrosome separation during spindle formation in vertebrates is intrinsic to each aster. J Cell Biol 122, 361–372.
Whitehead CM, Winkfein RJ, Rattner JB (1996). The relationship of HsEg5 and the actin cytoskeleton to centrosome separation. Cell Motil Cytoskeleton 35, 298–308.
Wittmann T, Hyman A, Desai A (2001). The spindle: a dynamic assembly of microtubules and motors. Nat Cell Biol 3, E28–E34.
Xiong F, Ma W, Hiscock TW, Mosaliganti KR, Tentner AR, Brakke KA, Rannou N, Gelas A, Souhait L, Swinburne IA, *et al.* (2014). Interplay of cell shape and division orientation promotes robust morphogenesis of developing epithelia. Cell 159, 415–427.